Liver INTERNATIONAL
OFFICIAL JOURNAL OF THE INTERNATIONAL ASSOCIATION FOR THE STUDY OF THE LIVER

Liver International ISSN 1478-3223

BASIC STUDIES

Oxidative stress rather than triglyceride accumulation is a determinant of mitochondrial dysfunction in *in vitro* models of hepatic cellular steatosis

Khalida A. Lockman[1], James P. Baren[2], Christopher J. Pemberton[2], Hussam Baghdadi[3], Karl E. Burgess[4], Nikolas Plevris-Papaioannou[2], Patricia Lee[2], Forbes Howie[3], Geoff Beckett[3], Anne Pryde[2], Alan J. Jaap[1], Peter C. Hayes[2], Celine Filippi[5] and John N. Plevris[2]

1 Department of Diabetes and Endocrinology, University of Edinburgh and Royal Infirmary of Edinburgh, Edinburgh, UK
2 Department of Hepatology, University of Edinburgh and Royal Infirmary of Edinburgh, Edinburgh, UK
3 Department of Clinical Biochemistry, University of Edinburgh and Royal Infirmary of Edinburgh, Edinburgh, UK
4 The Scottish Metabolomics Facility, University of Glasgow, Glasgow, UK
5 MRC Scottish Centre of Regenerative Medicine, University of Edinburgh, Edinburgh, UK

Keywords
mitochondrial dysfunction – *N*-acetylcysteine – nonalcoholic fatty liver disease – oxidative stress – reactive oxygen species – steatohepatitis

Abbreviations
AFU arbitrary fluorescent unit; CPT carnitine palmitoyl transferase; DMEM Dulbecco's Modified Eagle's Medium; DNP 2,4-Dinitrophenol; FFA free fatty acids; GPX1 glutathione peroxidase; HBSS Hank's buffered salt solution; LCFA long chain fatty acid; MCFA medium chain fatty acid; MEME minimal essential medium Eagle; NAC *N*-acetyl L-cysteine; NAFLD nonalcoholic fatty liver disease; PDH pyruvate dehydrogenase; ROS reactive oxygen species; TCA tricarboxylic acid; TR1 thioredoxin reductase; Δ_m mitochondrial membrane potential.

Correspondence
Dr Khalida Ann Lockman, Department of Diabetes and Endocrinology, Royal Infirmary of Edinburgh, 51, Little France Crescent, Edinburgh, EH16 4SA, UK
Tel: +0044 131 2421465
Fax: +0044 131 2421633
e-mail: k.a.lockman@sms.ed.ac.uk

Received 8 June 2011
Accepted 1 February 2012

DOI:10.1111/j.1478-3231.2012.02775.x

Abstract

Background/Aims: There is still debate about the relationship between fat accumulation and mitochondrial function in nonalcoholic fatty liver disease. It is a critical question as only a small proportion of individuals with steatosis progress to steatohepatitis. In this study, we focused on defining (i) the effects of triglyceride accumulation and reactive oxygen species (ROS) on mitochondrial function (ii) the contributions of triglyceride, ROS and subsequent mitochondrial impairment on the metabolism of energy substrates. *Methods:* Human hepatoblastoma C3A cells, were treated with various combinations of oleate, octanoate, lactate (L), pyruvate (P) and ammonia (N) acutely or for 72 h, before measurements of triglyceride concentration, cell respiration, ROS production, mitochondrial membrane potential, ketogenesis and gluconeogenesis, TCA cycle metabolite analysis and electron microscopy. *Results:* Acutely, LPON treatment enhanced mitochondrial respiration and ROS formation. After 72 h, despite the similarities in triglyceride accumulation, LPON treatment, but not oleate, dramatically affected mitochondrial function as evidenced by decreased respiration, increased mitochondrial membrane potential and ROS formation with concomitant enhanced ketogenesis. By comparison, respiration and ROS formation remained unperturbed with oleate. Importantly, this was accompanied by an increased gluconeogenesis and ketogenesis. The addition of the antioxidant *N*-acetyl-*L*-cysteine prevented mitochondrial dysfunction and reversed metabolic changes seen with LPON, strongly suggesting ROS involvement in mediating mitochondrial impairment. *Conclusions:* Our data indicate that ROS formation, rather than cellular steatosis *per se*, impairs mitochondrial function. Thus, reduction in cellular steatosis may not always be the desired outcome without concomitant improvement in mitochondrial function and/or reducing of ROS formation.

The growing diabetes and obesity pandemic are paralleled by a dramatic rise in the prevalence of nonalcoholic fatty liver disease (NAFLD). Characterized by intracellular triglyceride accumulation, NAFLD encompasses a spectrum of histological features ranging from simple steatosis that potentially, in the presence of inflammation, can progress to steatohepatitis, fibrosis and cirrhosis of the liver (1–3). Central to the development of dietary-induced NAFLD is enhanced energy substrates availability to the hepatocytes, which is often compounded by increased free fatty acids (FFA) flux tandem with hyperglycaemia. Within the hepatic

mitochondria, this leads to overproduction of the electron donors, NADH and $FADH_2$, fuelling the respiratory chain, thus potentially enhancing mitochondrial respiration and reactive oxygen species (ROS) formation. In turn, excessive ROS formation is thought to be the crux of molecular events leading to the development of hepatic insulin resistance and mitochondrial dysfunction (4–7). Indeed, altered mitochondrial function as evidenced by diminished respiratory chain activity and reduced ATP productions in steatohepatitis have been inextricably linked with oxidative stress (4, 5, 8–11).

Our study sought to address several fundamental questions on hepatic mitochondrial impairment in the presence of increased energy substrates. Firstly, enhanced energy substrates can potentially lead to cellular steatosis. The impact of cellular steatosis *per se* on mitochondrial function remains uncertain: does steatosis exert deleterious effects on mitochondrial function in the absence of ROS? Understanding the relationship between fat accumulation and mitochondrial function in NAFLD is a critical question as only a small proportion of individuals with steatosis progress to steatohepatitis. Secondly, although metabolic derangements have been closely associated with steatosis, the contributions of triglyceride, ROS and subsequent mitochondrial impairment on the metabolism of energy substrate remains unclear (5, 12). To elucidate the role of ROS (having found a combination of physiological substrates leading to higher ROS production in hepatocytes) we examined the effect of N-acetyl-L-cysteine, an antioxidant known to reduce cellular ROS. NAC has been shown to enhance mitochondrial function in adipocytes, cardiac and skeletal muscle (13–15). However, the effects of NAC on hepatic mitochondrial function and metabolic alterations associated with human steatohepatitis including enhanced ketogenesis (despite unaltered β-oxidation) and hepatic insulin resistance characterized by increased endogenous glucose production is not yet established (5).

To address these questions, we recapitulated the sequence of events proposed to occur in NAFLD using *in vitro* models. *In vitro* studies provide a controlled environment, independent of the influence exerted by adipocytokines and peripheral hyperinsulinaemia thus focusing on events that occur specifically in the hepatocytes. We used human hepatoblastoma C3A cells, treated with either oleate or octanoate to induce triglyceride accumulation. Medium chain free fatty acids (MCFA), such as octanoate, diffuse into mitochondria independently of carnitine palmitoyl transferase (CPT) thus allowing an exclusive and more efficient mitochondrial ß-oxidation than long chain fatty acids (LCFA)(16). A clonal derivative of hepatoblastoma-based HepG2 cell line, C3A cells, is selected for this study for its enhanced hepatic phenotype (17, 18). Furthermore, C3A cells had been previously used as a model for cellular steatosis (19). Lactate (L) and pyruvate (P), physiological substrates of both gluconeogenesis and de novo lipogenesis, were added to octanoate (O). The reasoning was that these energy substrates would synergistically enhance ATP turnover and mitochondrial respiration and promote significant intracellular lipid accumulation through de novo lipogenesis. The rate of respiration was further manipulated by adding ammonia to LPO with the hypothesis that the metabolism of ammonia by the urea cycle, or glutamine pathways would promote further NADH formation (20, 21).

Materials and methods

Cell culture

C3A cells (American Type Culture Collection, Manassas, VA, USA) were cultured in minimal essential medium Eagle (MEME) (Sigma, Dorset, UK) with 10% fetal calf serum (FCS) (Molecular Probes, Grand Island, NY, USA) and antibiotics (100 IU/ml penicillin, 100 mg/ml streptomycin) (Invitrogen, Grand Island, NY) at 37°C and 5% CO_2, until 70% confluent. The media was then supplemented with combinations of octanoate (O) (2 mM) or oleic acid (Ol) (0.25 mM) complexed with bovine serum albumin (BSA), lactate (L) (10 mM), pyruvate (P) (1 mM) with or without ammonia (N) (4 mM). Cells were cultured in the supplemented media using the concentrations stated above for 72 h (unless specified) prior to experimentation.

BODIPY 493/503 lipid staining and triglyceride quantification

Cells were pretreated on chamber slides and fixed with 4% paraformaldehyde (Sigma) for 30 min before staining with 200 μl of BODIPY 493/503 (Invitrogen) for 10 min. Cells were mounted in coverslips using ProLong® gold antifade reagent (Invitrogen). Slides were left for 24 h at 4°C before viewed using confocal laser microscope (LSM510; Carl Zeiss MicroImaging, Inc., Hertfordshire, UK). Fluorescence intensity in at least 50 cells per image was analysed using ImageJ software (National Institutes of Health, Bethesda, MD, USA). Triglyceride quantification was performed using a triglyceride assay kit (Thermo Electron, Louisville, CO, USA) adapted for the Cobas FARA (Roche Diagnostics Ltd, Welwyn Garden City, UK).

Quantification of mitochondrial superoxide production

Mitochondrial superoxide production was measured using the live-cell permeable fluorescent probe MitoSOX™ Red (Invitrogen). MitoSOX™ stock solution was prepared according to protocol specified by the manufacturer. For fluorescent microscopy, naïve C3A cells grown in two-chamber slides were incubated with MitoSOX™ for 45 min. The supernatant was then removed and cells were rinsed, before the addition of 500 μl of HBSS with or without specified combination

of the energy substrates into each chamber. Images were obtained using fluorescent microscopy (LSM510; Carl Zeiss MicroImaging, Inc.). Phase contrast and fluorescent images were merged using image editor software, Photoshop CS4 (Adobe Systems Incorporated, San Jose, CA, USA). Fluorescence intensity from each image was analysed using ImageJ (National Institutes of Health). For quantification of superoxide using FACS, trypsinized cells were suspended in 5 μM MitoSOX^{TM} solution at 37°C for 45 min. Cells were then resuspended in HBSS (to determine superoxide formation with basal respiration) or in LPON (to examine superoxide formation with substrate driven respiration) before FACS (FACS Calibur^{TM}; BD Biosciences, San Jose, CA, USA).

Enzyme activity assay for glutathione peroxidase 1 (GPX1) and thioredoxin reductase (TR1) concentration

To investigate the induction of selenoenzymes, such as TR1 and GPX1, it is imperative to develop selenium-deficient media without affecting cell viability. Thus, for these experiments, C3A cells were maintained in Dulbecco's Modified Eagle's Medium (DMEM; 4.5 g/L glucose; Lonza Ltd, Basel, Switzerland) containing 10% FBS, L-glutamine (2 mM), (Lonza), penicillin (100 IU/ml), streptomycin (100 mg/ml), amphotericin B (250 ng/ml); (Lonza), sodium pyruvate (1 mM) (Cambrex, East Rutherford, NJ, USA). After 24 h, cells were rinsed in phosphate-buffered saline (PBS) then conditioned in DMEM supplemented with 10 mg/L transferrin (Sigma-Aldrich Company Ltd, Poole, Dorset, UK) and 10 mg/L insulin (Autogen Bioclear, Calne, Wiltshire, UK) resulting in selenium content of <0.13 nM (as determined by The Scottish Trace Element and Micronutrient Reference Lab, Dept. Clinical Biochemistry, Royal Infirmary Glasgow). After 24 h, cells were rinsed with HBSS before treatment with oleate at 0.25 mM or 0.5 mM or palmitate at 0.125 mM or 0.25 mM in DMEM supplemented with insulin and transferrin for 24 h. Treatment duration was chosen based on the observation that maximal triglyceride accumulation with oleate (0.25 mM) occurred at 24 h. Assays for glutathione peroxidase 1 (GPX1) activity and thioredoxin reductase 1 (TR1) concentrations were performed using Cobas-Fara centrifugal analyzer using method previously described (22).

Determination of membrane potential

Treated C3A cells were labelled with 5 μM of JC-1 (Molecular Probes) for 20 min at 37°C as adherent cells before trypsinization and analysed with FACS (FACS Calibur^{TM}; BD Biosciences).

Mitochondrial respiration

For acute mitochondrial respiration, 0.5×10^6 naïve confluent C3A cells in single suspension were treated with oleate or octanoate with the combination of lactate, pyruvate and/or ammonia. Oxygen consumption was analysed using BD^{TM} Oxygen Biosensor 96-well plate (BD Biosciences). To analyse respiration after a 72-h treatment, treated cells were added to the following media; Hank's buffered salt solution (HBSS), HBSS with LPON, or HBSS with LPON and 2,4-Dinitrophenol (DNP) (250 μM). The fluorescent plates were read in CytoFluor Reader Series 4000 (MTX Lab Systems, Vienna, VA, USA) for 40 min. The respiration rates were measured from the linear portion of the slope of fluorescence rise. Data are presented as arbitrary fluorescent units (AFU) or as fold of change from the untreated cells.

Protein quantification

Cellular protein was quantified using BCA protein assay reagent (Pierce Biotechnology, Rockford, IL, USA) according to manufacturer's instructions.

Metabolomics profiling of TCA cycle intermediates

Cells were centrifuged (1000*g*) for 10 min at 37°C. The cell pellet was resuspended in 1 ml of supernatant, transferred to a 1.5 ml tube, and the final pellet was obtained by further centrifugation (3000*g*) for 5 min followed by a complete removal of supernatant. Metabolites were extracted from the cell pellet by the addition of 200 μl of chloroform/methanol/water (1:3:1) with vigorous mixing for 1 h at 4°C. Precipitated proteins and cellular debris were removed by centrifugation (13 000*g*) for 5 min. Supernatant was kept at −80°C until LC-MS analysis within 2 weeks. Additional control samples included cell-free growth medium and extraction solvent served as blanks.

The LC separation was performed using hydrophilic interaction chromatography with a ZIC–HILIC 150 × 4.6 mm, 5 μm column (Merck Sequant, Umeå, Sweden), operated by an UltiMate 3000 RSLC liquid chromatography system (Dionex, Camberley, Surrey, UK). The separation consisted of a linear gradient from 80% B to 20% B over 30 min, followed by an 8-min wash with 5% B, and 8-min reequilibration with 80% B, where solvent B was 0.08% formic acid in acetonitrile, and solvent A was 0.1% formic acid in water. The flow rate was 300 μl/min, column temperature 20°C, injection volume 10 μl, and samples were maintained at 4°C. The mass spectrometry was performed using an Orbitrap Exactive (Thermo Fisher Scientific, Hemel Hempstead, UK) with a HESI 2 probe. The spectrometer was operated in polarity switching mode, with the following settings: resolution 50 000, m/z range 70–1400. Ionization voltages were +4.5 and –3.5 kV in positive and negative modes respectively.

Raw LC-MS data were processed with a combination of XCMS Centwave for peak picking (http://mzmatch.sourceforge.net/), and mzMatch for alignment and

annotation of related peaks (http://mzmatch.sourceforge.net/). Metabolite identification was performed by matching masses and retention times to the database with mass accuracy window of 3 ppm (if two formulae were within 3 ppm the closest match was taken) and RT window of 35% (by in-house VBA scripts). Additional automated noise and MS artefact filtering procedures were applied to remove peak sets that contained: (i) peaks that were present at equal or higher abundance in the blank solvent samples, (ii) all peaks lower than the intensity threshold (10 000), (iii) shoulder peaks or duplicate peaks within the same mass (3 ppm) and retention time (0.2 min) window, (iv) common MS artefacts, (v) irreproducible intensities (relative standard deviation >0.5) across replicate samples.

Determination of ketogenesis, mitochondrial and cytosolic ratios and glucose concentration

For ketogenesis, β-hydroxybutyrate and acetoacetate concentrations in each cell culture medium were measured immediately after the 72-h treatment using Bergmeyer's enzymatic methods (23). Mitochondrial and cytosolic NADH/NAD^+ ratios were determined using the ratio of β-hydroxybutyrate to acetoacetate, and lactate to pyruvate respectively. Because the concentrations of lactate and pyruvate in the culture supernatant would preclude a conclusive determination of cytosolic NADH/NAD+ ratio, the treated cells were rinsed and allowed to reach a steady state for 24 h in MEME prior to a 4-h incubation with PBS and octanoate (2 mM). Lactate, pyruvate, β-hydroxybutyrate and acetoacetate concentrations in the incubation medium was measured using Bergmeyer's enzymatic methods (23). For glucose formation, treated cells from all groups were rinsed before a 4-h incubation with further LPON. Glucose concentration was then measured in the incubation medium using Bergmeyer's enzymatic methods (23).

Electron microscopy

Cells were centrifuged to form pellets in the fixative (3% glutaraldehyde in 0.1 M sodium cacodylate buffer, pH 7.3) then washed in three 10-min changes of 0.1 M sodium cacodylate. Specimens were then post-fixed in 1% osmium tetroxide in 0.1 M sodium cacodylate for 45 min, and washed in three 10-min changes of 0.1 M sodium cacodylate buffer. Samples were dehydrated in 50, 70, 90 and 100% normal grade acetones for 10 min each, then for a further two 10-min changes in analar acetone. Samples were embedded in Araldite resin. Sections, 1 μm thick, were cut on a Reichert OMU4 ultramicrotome (Leica Microsystems (UK) Ltd, Milton Keynes, UK), stained with toluidine Blue and viewed in a light microscope. Ultrathin sections, 60 nm thick were cut from selected areas, stained in uranyl acetate and lead citrate before viewed in Phillips CM120 Transmission electron microscope (FEI UK Ltd, Cambridge, UK). Images were taken using Gatan Orius CCD camera (Gatan UK, Abingdon, UK).

Cell viability

Cell viability was assessed as the percentage retention of lactate dehydrogenase (LDH) by the cell using LDH kit (Alpha Laboratories, Hampshire, UK) modified for use on the Cobas-Fara analyzer as described previously (22). The results are expressed as percentage LDH activity retained.

Statistics

Statistical analyses were performed using GraphPad Prism® (GraphPad Software, La Jolla, CA, USA). Results were expressed as mean ± standard error of the mean (SEM) unless specified. Differences between groups were compared with one-way ANOVA with Newman–Keuls multiple comparison analysis. For triglyceride accumulation, two-way ANOVA was performed to determine the interaction between the specified treatment and the duration of treatment. A value of $P < 0.05$ was considered as statistically significant. Unless stated otherwise, experiments were done to at least $n = 3$ in triplicate.

Results

LPON acutely increases mitochondrial respiration and superoxide formation

We postulated that the combination of lactate, pyruvate and ammonia would act synergistically with octanoate to enhance mitochondrial respiration. To test this hypothesis, treatment media were added to naïve C3A cells before the measurements of cell respiration using BD Biosensor. LPO resulted in a 2.5-fold rise in respiration whereas LPON resulted in a three-fold increment when compared with the untreated groups (Fig. 1A). Next, we examined whether the rise in respiration with LPON is paralleled by an increase in mitochondrial superoxide formation. Naïve C3A cells grown in chamber slides were incubated with MitoSOX™ (Invitrogen). Cells were rinsed before adding HBSS with or without LPON. DNP (250 μM) or oligomycin (5 μg/ml) were added to HBSS in additional chambers, as controls. Oligomycin, a classic ATP synthase inhibitor, dramatically increases the mitochondrial membrane potential by preventing the reentry of protons in the mitochondrial matrix, thus leading to the respiratory chain complex electron slip and superoxide formation. In contrast, the uncoupler, protonophore 2,4-dinitrophenol (DNP), lowers mitochondrial membrane potential and reduces superoxide production. Figure 1B–E show representative images obtained from fluorescent microscopy. Superoxide formation (fluoresced in bright red) was visibly enhanced in LPON and oligomycin. Figure 1F

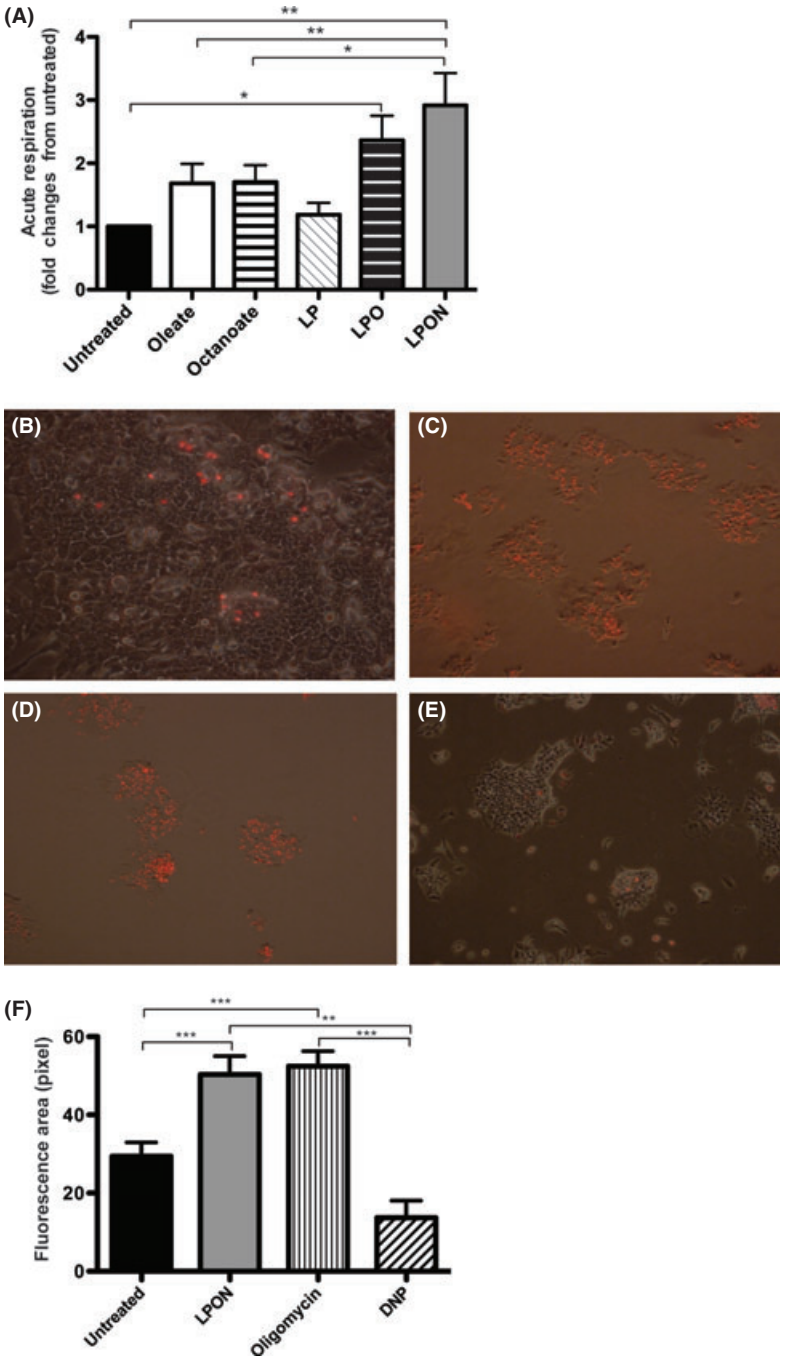

Fig. 1. The acute effects of energy substrates on (A), cell respiration (B)–(F), reactive oxygen species (ROS) formation in naïve C3A cells. (A) For acute cell respiration, naïve C3A cells in single suspension were used for each well of the BD Biosensor fluorescent plate containing one of the following media: HBSS with oleate (0.25 mM) or specified combinations of lactate (L) (10 mM), pyruvate (P) (1 mM), octanoate (O) (2 mM) and ammonia (N) (4 mM). Cell respiration was calculated from the slope of the linear section of the curve representing the fluorescent intensity ($P = 0.0008$, $*P < 0.05$, $**P < 0.01$). (B–F) Mitochondrial superoxide formation with acute LPON treatment viewed under fluorescent microscopy after a 45-min incubation with MitoSOX^{TM}. Naïve C3A cells were grown in two-chamber slides. Cells were rinsed before being treated with 500 μl of HBSS, HBSS+LPON, HBSS+DNP (250 μM) and HBSS+oligomycin (5 μg/ml) into each chamber. Oligomycin increases mitochondrial membrane potential ($\Delta\Psi m$) thus augmenting the leakage of electrons resulting in superoxide formation from the mitochondrial respiratory chain. In contrast, 2,4-dinitrophenol (DNP) lowers $\Delta\Psi m$, hence diminishing the rate of superoxide production by mitochondria. Panel (B)–(E) are fluorescent images viewed under fluorescent microscopy (magnification ×10). (B), Untreated; (C), LPON; (D), Oligomycin; (E), DNP; (F), Fluorescent area from each image analysed by ImageJ. Data are expressed in pixel, and represent mean ± SEM, $P < 0.0001$; $**P < 0.01$; $***P < 0.001$.

shows that LPON had higher fluorescence intensity than the untreated cells. Furthermore, fluorescence intensity with LPON was similar to that seen with oligomycin and was significantly higher than that of DNP.

Cellular steatosis and triglyceride concentrations

Next, we investigated whether incubation with substrates that acutely modulate ROS formation resulted in cellular steatosis, a cardinal feature of human NAFLD. C3A cells were incubated with the different combinations of energy substrates for 72 h. Intracellular lipid vacuoles visible under electron microscopy (Fig. 2A) were confirmed by BODIPY 493/503 staining (Fig. 2B and C). Pretreatment with oleate, octanoate and LPON induced higher intracellular lipid accumulation than seen in the untreated cells (Fig. 2C). To quantify the steatotic effects of each treatment group, triglyceride concentrations were measured. As shown in Figure 2D, the pattern of triglyceride accumulation over time was significantly different between the oleate and octanoate-treated cells. Oleate induced higher triglyceride concentrations in the first 24 h, but subsequently reached a plateau. In contrast, triglyceride concentration with octanoate increased with time potentially reflecting de novo lipogenesis from acetyl-coA formed with recurring

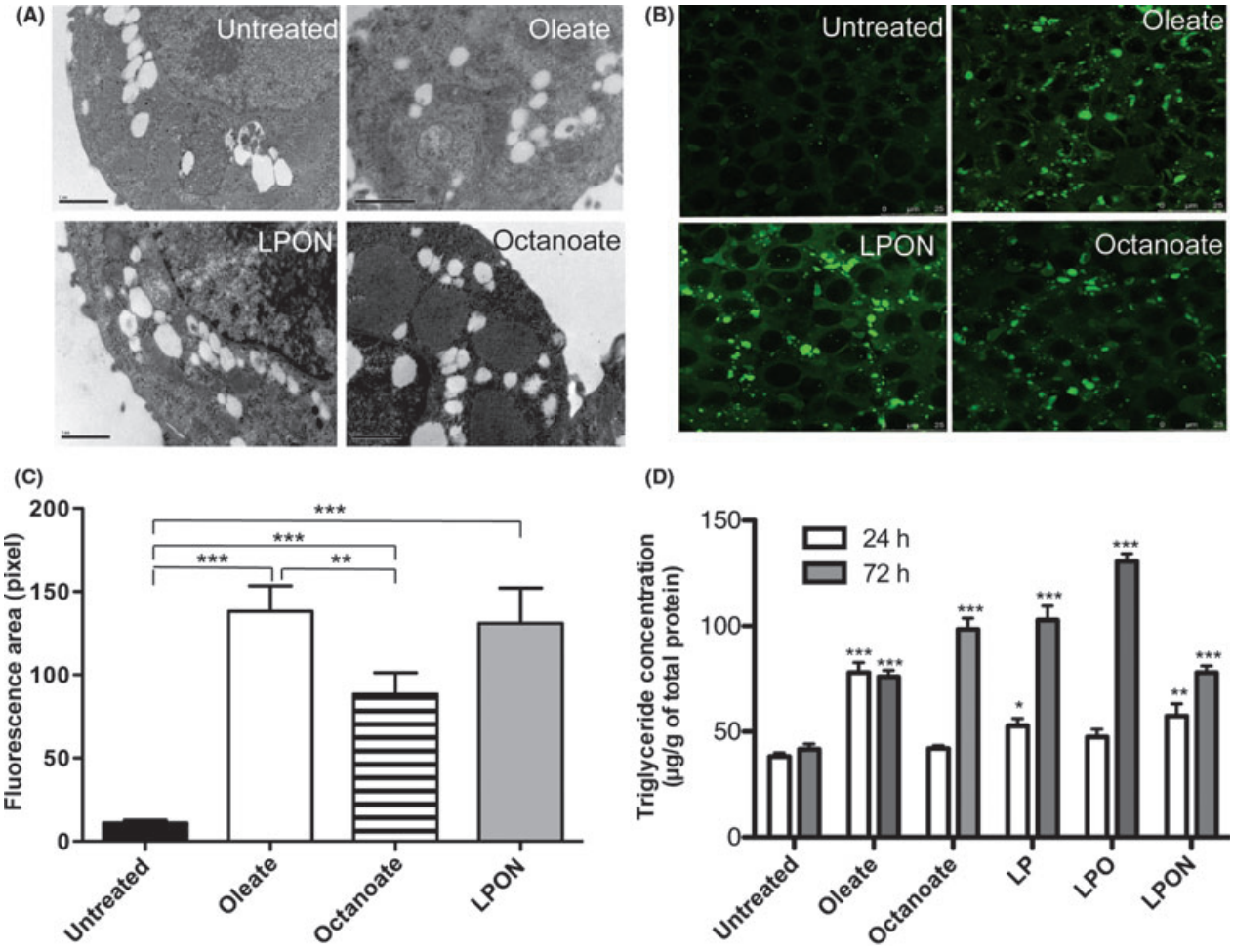

Fig. 2. Triglyceride accumulation in treated C3A cells. (A) Transmission electron microscopy demonstrating the presence of lipid droplets (B) BODIPY 493/503 staining confirming the presence of lipid accumulation (C) Fluorescence area from BODIPY 493/503 staining (D) Triglyceride concentrations after 24 and 72 h of treatment. C3A cells were treated for 72 h (unless specified) with various combinations of energy substrates. (A) Transmission electron microscopy demonstrated the presence of lipid droplets in cells treated with oleate, LPON and octanoate (scale bar on the micrographs represents 1 μm). (B) The presence of lipid was confirmed with BODIPY 493/503 staining, which renders the lipid droplets bright green fluorescence (scale bar represents 25 μm). (C) Fluorescence area from BODIPY 493/503 staining was quantified using ImageJ. $^{**}P < 0.01$; $^{***}P < 0.001$; data are presented as means ± SEM. (D) Triglyceride concentrations were measured after 24 or 72 h of treatment. $P < 0.0001$ for interaction between treatment and duration of treatment (determined by two-way ANOVA). $^{***}P < 0.001$, $^{**}P < 0.01$ and $^{*}P < 0.05$ compared with untreated cells of the same treatment duration; $n = 3$ in triplicates. Data presented are mean ± SEM.

sequence of β-oxidation rather than direct esterification. All treatment groups induced significant triglyceride accumulation when compared with untreated cells after 72 h. The synergistic effect of lactate, pyruvate and octanoate (LPO) resulted in higher triglyceride accumulation than that seen with either LP ($P < 0.001$) or octanoate alone ($P < 0.001$). Triglyceride concentrations with LPON after 72 h were 40% lower than seen with LPO ($P < 0.001$), but were similar to that accrued with oleate (Fig. 2D). As NAC has been shown to modulate ROS in a number of studies, we also studied its effects when combined to LPON (13, 24). The addition of NAC (10 mM) to LPON throughout the 72-h pretreatment did not alter triglyceride concentration (LPON 235.3 ± 12.2 vs. LPON+NAC 237.3 ± 7.2 μg/g of total protein, $P = 0.9$, $n = 5$ in triplicates).

Cell viability

The LPON treatment did not affect cell viability after 72 h as evidenced by LDH retention (LPON 97.9 ± 0.33, oleate 98.2 ± 0.32, untreated 98.3 ± 0.39% LDH activity retained; $P = 0.63$).

Cellular steatosis alone does not result in mitochondrial dysfunction

Given the similarities in triglyceride accumulation with LPON and oleate, the impact of cellular steatosis on mitochondrial respiration was focused on these groups. As shown in Figure 3A, oleate and untreated cells had a similar basal respiration, despite contrasting triglyceride accumulation. Furthermore, whilst acute exposure with LPON results in increased cell respiration, the 72-h LPON treatment led to a significantly lower basal respiration compared with the oleate or the untreated cells (Fig. 3A). Concomitant treatment with antioxidant, NAC or α-tocopherol (0.4 mM), prevented the decrease in basal respiration in LPON treated cells. Respiration was 62 and 53% higher in LPON cells treated simultaneously with NAC or α-tocopherol, respectively, when compared with LPON alone (Fig. 3A). To examine the

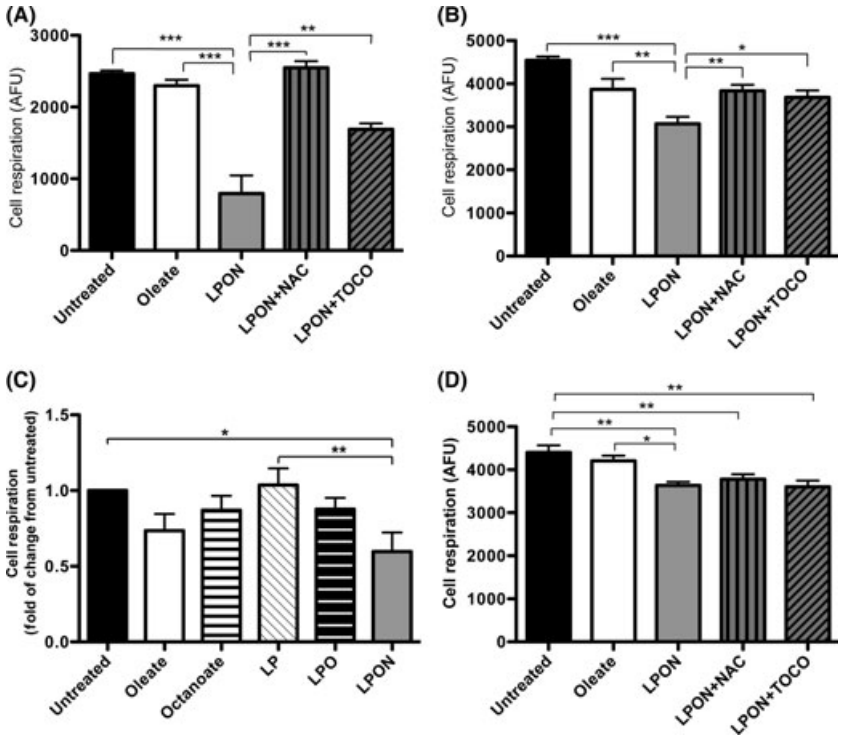

Fig. 3. C3A cell respiration after a 72-h treatment. (A) Respiration in treated C3A cells suspended in HBSS (B) Respiration in cells suspended in HBSS+LPON (C) Respiration in treated cells suspended in HBSS+LPON+uncoupling agent 2,4 dinitrophenol (DNP) (D) Respiration in cells treated simultaneously with NAC and α-tocopherol in the presence of LPON+DNP (A) Cell respiration in the treated cells was measured using BD Oxygen Biosensor. Besides oleate and LPON, N-acetylcysteine (10 mM) or α-tocopherol (0.4 mM) were added to LPON throughout the treatment period. Cell respiration was calculated from the linear section of the slope for fluorescence increase. Data are presented in mean ± SEM, $P < 0.0001$; $^{**}P < 0.01$; $^{***}P < 0.001$. (B) To examine substrate-driven respiration and to confirm the presence of intact intermediary metabolism, respiration was measured in treated cells suspended in HBSS+LPON; $P < 0.0001$; $^{*}P < 0.05$; $^{**}P < 0.01$; $^{***}P < 0.001$. (C) LPON+DNP was added to all groups. Data are presented as fold of change from the untreated cells, $P = 0.003$, $^{*}P < 0.05$; $^{**}P < 0.01$. (D) N-acetylcysteine (10 mM) or α-tocopherol (0.4 mM) was added to LPON throughout the treatment period. Respiration was then measured in the presence of DNP. Data are presented in mean ± SEM and expressed as arbitrary fluorescent unit (AFU). $P = 0.0009$, $^{*}P < 0.05$; $^{**}P < 0.01$.

impact of triglyceride accumulation on substrate-driven respiration, HBSS containing LPON was added to all groups immediately before measurement of cell respiration. All groups demonstrated increased respiration with the addition of further substrates (Fig. 3B). However, respiration for the LPON-treated cells remained lower than seen with the untreated cells. The combination of LPON with NAC or α-tocopherol restored the cell respiration by 25 and 20%, respectively, when compared with LPON treatment alone (Fig. 3B). To examine the maximal capacity of mitochondrial respiratory chain, DNP was added to all treated groups. In the presence of DNP, the rise in cell respiration was significantly lower with the LPON-treated cells when compared with the untreated cells, suggesting decreased mitochondrial respiratory chain capacity. In contrast, the rise in respiration induced by DNP for oleate, octanoate, LP and LPO groups were comparable to that seen with the control cells (Fig. 3C), showing an overall lack of impact on the respiratory chain under these conditions. Interestingly, neither NAC nor α-tocopherol significantly improved the respiration in LPON treated cells (Fig. 3D).

Superoxide formation is sustained in LPON cells despite a reduction in respiration

Next, we investigated the impact of altered cell respiration on superoxide formation. Figure 4A shows mitochondrial superoxide formation during basal respiration after a 72-h treatment. Despite reduced basal respiration with LPON when compared with the control cells (Fig. 3A), superoxide formation was similar in these groups (Fig. 4A). Figure 4B represents superoxide formation capacity during substrate-induced respiration. Here, cells incubated with MitoSOX^{TM} (Invitrogen) were resuspended in LPON prior to FACS. A two-fold rise in mitochondrial superoxide formation was observed in LPON when compared with the untreated cells (Fig. 4B). In contrast, mitochondrial superoxide formation in oleate remained similar to that seen in untreated cells (Fig. 4B). As ROS formation in mitochondria is modulated by the mitochondrial membrane potential ($\Delta\Psi_m$) as well as the redox potential (25, 26), we next chose to analyse the $\Delta\Psi_m$ and the NADH/NAD$^+$ in oleate, LPON and LPON+NAC-treated cells. Using JC-1 fluorescence analysis, $\Delta\Psi_m$ was determined in cells treated for 72 h (Fig. 4C). Although oleate treated cells had similar $\Delta\Psi_m$ to the untreated group, LPON treated cells showed higher mitochondrial membrane potential. Concomitant treatment with LPON and NAC led to a lower $\Delta\Psi_m$ when compared with cells treated with LPON alone (Fig. 4C). Despite their disparity in ROS formation, mitochondrial NADH/NAD$^+$ ratio with LPON was similar to that seen with the untreated cells. In contrast, mitochondrial NADH/NAD$^+$ ratio was significantly higher with LPON compared with oleate (Fig. 4D). Figure 4E shows that cytosolic NADH/NAD$^+$ ratio was higher in LPON than the untreated cells.

Altered flux of energy substrates and TCA cycle activity

To investigate whether mitochondrial respiration impairment alters metabolic fluxes into the TCA cycle, the rate of ketogenesis was determined after a 72-h treatment. In the presence of reduced TCA activity, acetyl-coA is diverted towards ketogenesis instead of entering the TCA cycle. Figure 5A shows higher ketogenesis with LPON than the untreated cells. Co-treatment of LPON+NAC led to a considerable reduction in ketogenesis by 41% when compared with LPON alone suggesting possible reduced TCA cycle turnover in LPON treated cells and the potential involvement of ROS in this process (Fig. 5A). To further determine the impact of each treatment on TCA cycle activity, we conducted the profiling of TCA cycle metabolites. Using the metabolomics approach, four metabolites that correspond to TCA cycle intermediates were identified. As shown in Figure 5B, the quantity of citrate was lower with LPON than that seen with oleate. All groups had similar levels of cis-aconitate and succinate (Fig. 5C and D). The higher concentration of malate with LPON when compared with the untreated cells is consistent with the reduction of oxaloacetate to malate, which has been shown to occur in the presence of high concentration of acetyl-CoA (Fig. 5E) (27).

Higher glucose formation in LPON-treated cells is reversed by concomitant treatment with NAC

Next, we examined the relationship between mitochondrial dysfunction, oxidative stress and glucose production. Figure 6 represents glucose formation in the incubation media after a 4-h incubation with LPON. The rate of glucose formation with LPON remained higher than that seen with oleate or the untreated cells. Interestingly, despite the similarities in their effect on mitochondrial respiratory chain capacity, octanoate treatment led to a higher glucose fluxes than oleate suggesting that altered glucose metabolism may precede mitochondrial impairment. LPON+NAC resulted in a significant reduction of 43% in glucose flux when compared with LPON alone (Fig. 6).

Triglyceride accumulation with oleate is not associated with increased antioxidant thioredoxin reductase (TR1)

To confirm that the marked differences observed between oleate and LPON are not attributable to enhanced cytoprotective effect with oleate, we measured TR1 concentrations in oleate treated cells after maximal triglyceride accumulation has been achieved at 24 h. Oleate induced steatosis had been shown to increase cellular reduced glutathione (GSH) content accompanied by enhanced lipid peroxidation (28). 4-Hydroxynonenal

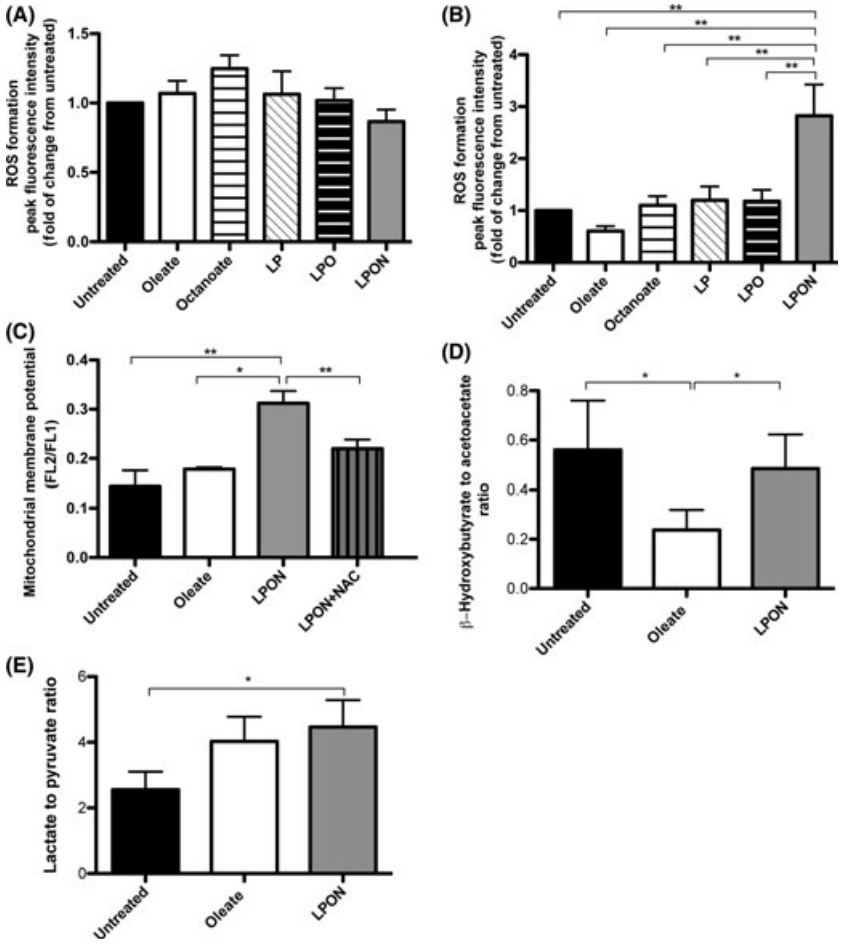

Fig. 4. Mitochondrial superoxide formation in treated C3A cells after 72 h. (A) Mitochondrial superoxide formation during basal respiration (B) Superoxide formation during substrate driven respiration (C) Mitochondrial membrane potential ($\Delta\Psi$m), (D) Mitochondrial NADH to NAD^+ ratio (E) Cytosolic NADH to NAD^+ ratio. (A) To quantify superoxide formation, cells were trypsinized and incubated with MitoSox™. Cells were resuspended in HBSS before FACS analysis; $P = 0.25$. (B) To determine superoxide formation during substrate driven respiration, cells were incubated with MitoSox™ as described previously and were resuspended in LPON; $P < 0.0001$; $^{**}P < 0.01$, (C) Treated cells from each group were incubated with fluorescent cationic dye, JC-1 for 20 min then trypsinized before FACS. JC-1 fluoresces in green in cells with low $\Delta\Psi_m$ and forms aggregated that fluoresce in red within high $\Delta\Psi_m$ mitochondria. Hence, the level of mitochondrial potential can be evaluated by calculating the ratio of median intensity of red (detected in FL2 channel) to green (detected in FL1 channel). Data are presented in mean ± SEM, $P = 0.003$, $^{*}P < 0.05$; $^{**}P < 0.01$. LPON+NAC; LPON+N-acetylcysteine. LPON+TOCO, LPON+α-tocopherol. (D) To determine mitochondrial NADH to NAD^+ ratio, treated cells were rinsed and the culture medium is replaced with MEME for 24 h before a 4-h incubation with PBS and octanoate. The concentrations of β-hydroxybutyrate and acetoacetate were then measured in the incubation medium to determine (β-hydroxybutyrate to acetoacetate ratio). Data are presented in mean ± SEM, $P = 0.03$; $^{*}P < 0.05$. (E) cytosolic NADH to NAD^+ ratio (lactate to pyruvate ratio) was determined from lactate and pyruvate concentrations in the incubation medium following a 4-h incubation with PBS and octanoate as described above. Data shown are mean ± SEM, $P = 0.04$; $^{*}P < 0.05$.

(4-HNE), a major end-product of lipid peroxidation can potentially exert cytoprotective effect primarily through the induction of thioredoxin reductase 1 (TR1) (29). Increased concentration of TR1 and enhanced activity of selenoenzyme, GPX1, can occur with oxidative stress (30, 31). Here, we also included cells treated with palmitate, a long chain fatty acid known to induce significant oxidative stress in hepatocytes (24). Figure 7A demonstrates triglyceride concentrations in each group. Figure 7B shows that TR1 concentrations were similar in oleate and palmitate treated cells. Similarly, the levels of GPX and TR1, which are crucial for peroxide reduction, were largely unaltered with individual treatment with lactate, pyruvate or ammonia (Fig. 7C and D).

Discussion

In the present study, we have designed *in vitro* models of cellular steatosis using various combinations of physiological energy substrates that are relevant to human dietary nonalcoholic fatty liver disease. As evidenced by

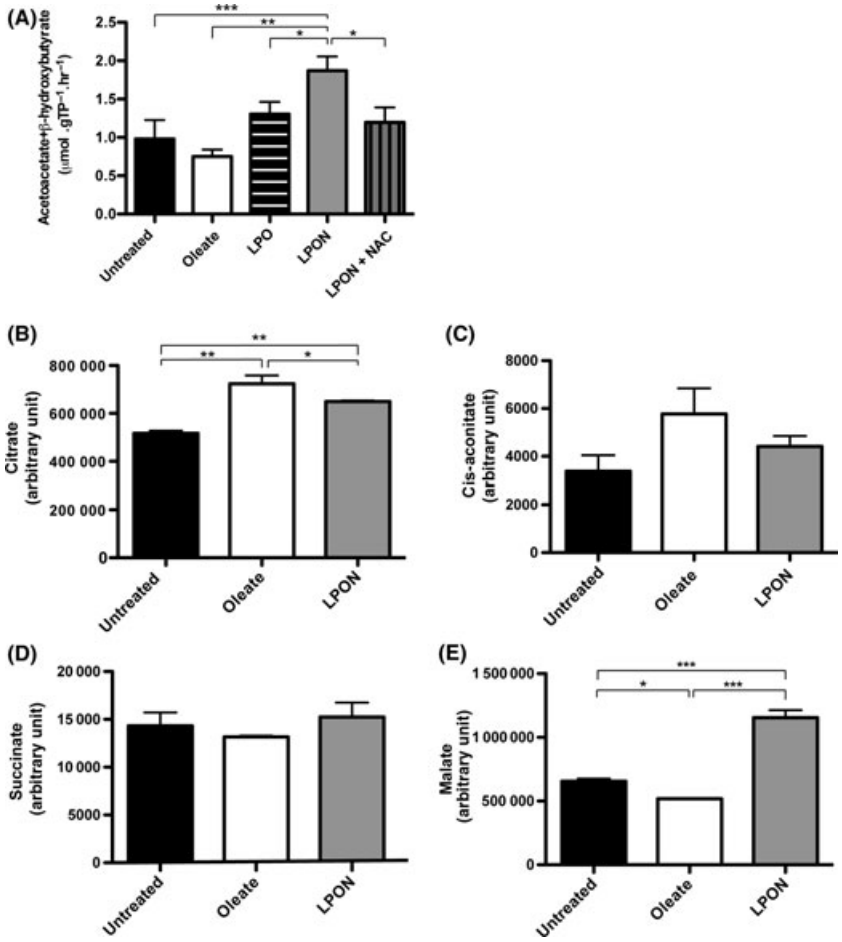

Fig. 5. Ketogenesis and TCA cycle activity in treated C3A cells after 72 h. (A) Ketogenesis determined from the total β-hydroxybutyrate and acetoacetate concentrations (B)–(E), TCA cycle intermediates identified using the metabolomics approach. (A) β-hydroxybutyrate and acetoacetate concentrations in the supernatant were measured after 72 h to determine the rate of ketogenesis. Data are presented in mean ± SEM and are expressed in μmol per gram of total protein per hour; $P = 0.001$, $*P < 0.05$; $**P < 0.01$; $***P < 0.001$. (B) Citrate ($P = 0.001$, $*P < 0.05$; $**P < 0.01$) (C) Cis-aconitate ($P = 0.16$) (D) Succinate ($P = 0.51$) and (E) Malate ($P < 0.001$, $*P < 0.05$, $***P < 0.001$) as quantified using metabolomics described in *methods*. Data are presented in mean ± SD and are expressed in arbitrary unit.

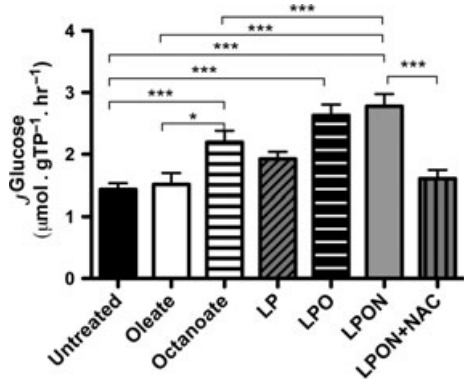

Fig. 6. Gluconeogenic capacity in treated C3A cells. Treated cells were rinsed before a 4-h incubation with LPON to determine glucose formation. Glucose flux was determined at the end of a 4-h incubation period. $P < 0.0001$, $*P < 0.05$, $***P < 0.001$. Data presented are mean ± SEM. LPON+NAC; LPON+N-acetylcysteine.

the differences in their mitochondrial respiration, fatty acids oleate or octanoate, with or without the combination of gluconeogenic substrates (lactate and pyruvate), and/or ammonia acutely modulated the TCA cycle turnover. The focus was then to observe the events that occur as consequences of enhanced TCA activity similar to what potentially may occur with nutrient excess. Our aims were to determine (i) whether steatosis *per se* affects mitochondrial respiration and (ii) whether its effects are essentially hinged on ROS formation. We have shown that lactate, pyruvate, octanoate and ammonia synergized to enhance respiration and ROS formation to a critical point, culminating in mitochondrial impairment. Indeed, LPON-induced cellular steatosis manifests many of the key features associated with steatohepatitis, such as impaired mitochondrial function, enhanced oxidative stress, increased ketogenesis and altered glucose metabolism. In stark contrast, triglycer-

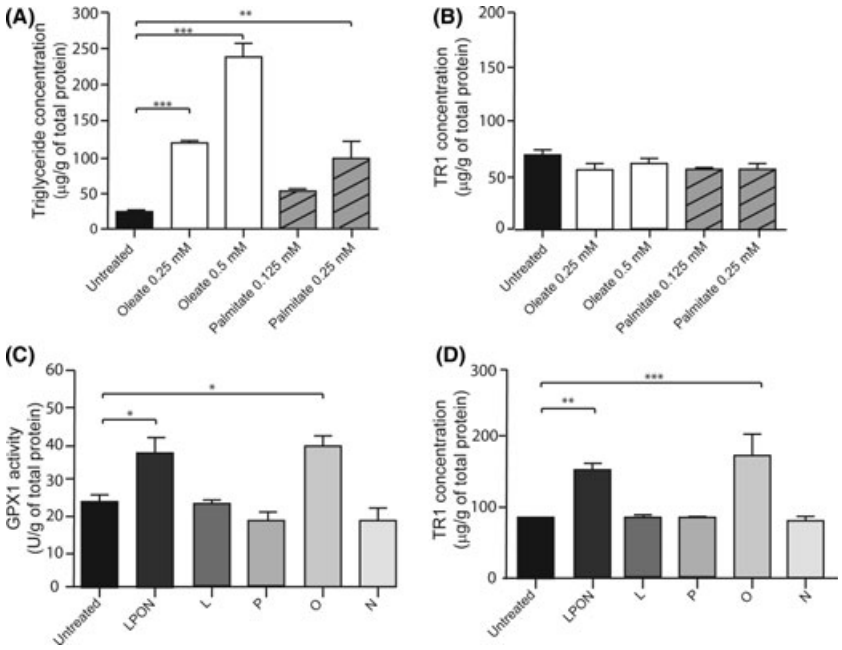

Fig. 7. Maximal triglyceride accumulation induced by oleate is not associated with increased antioxidant thioredoxin reductase 1 (TR1) (A) Triglyceride concentrations in oleate and palmitate treated cells. (B) TR1 concentrations in oleate and palmitate treated cells (C) GPX1 activity in individual component of LPON, (D) TR1 concentration in each LPON component. (A) We observed that maximal triglyceride accumulation with oleate was achieved after 24 h. Thus, for this series of experiment, cells were pretreated with either oleate (0.25 and 0.5 mM) or palmitate (0.125 and 0.25 mM) for 24 h. *$P < 0.05$, **$P < 0.01$; ***$P < 0.001$, data represent mean ± SEM. (B) Intracellular TR1 concentrations were determined in cells were pretreated with either oleate or palmitate at the concentration specified for 24 h, *$P < 0.05$,**$P < 0.01$; ***$P < 0.001$, data are presented as mean ± SEM. (C) The activity of GPX1 and (D) TR1 levels were determined for individual component of LPON after 48 h, *$P < 0.05$, **$P < 0.01$; ***$P < 0.001$, data are presented as mean ± SEM.

ide accumulation with oleate represents simple steatosis; mitochondrial function remained unperturbed despite the triglyceride accrued.

Our data have several important implications for understanding the events surrounding mitochondrial dysfunction in nutrient perturbation. Firstly, cellular steatosis *per se* does not influence mitochondrial function. In support of this, mitochondrial function was significantly different between oleate and LPON despite their similarities in triglyceride accumulation. Enhanced respiration with LPON was not sustained; evidence of mitochondrial impairment was apparent after 72 h as supported by decreased basal and substrate-driven respiration as well as diminished mitochondrial chain capacity. Likewise, mitochondrial function remained unaltered with LPO despite higher intracellular triglyceride accumulation when compared with LPON. There are two potential mechanisms behind the lower triglyceride content with LPON when compared with LPO treated cells. Firstly, impaired mitochondrial function would lead to ATP depletion, thus switching off ATP-consuming processes including de novo lipogenesis. Indeed, downregulation of lipogenic enzymes has been proposed to be the mechanism of decreased steatosis or 'burnt out' appearances in advanced NASH (32). Secondly, ammonia has been shown in astrocytes to decrease the formation of triglycerides with concomitant rise in diacylglycerides, further supporting the importance of triglycerides in protecting cells from the potential deleterious effect of free fatty acids (33, 34).

Secondly, our data underlines the importance of energy substrates capacity to form ROS, rather than their ability to induce triglyceride accumulation, as a key determinant of mitochondrial function. We have shown that LPON treatment acutely enhanced ROS formation culminating in increased mitochondrial membrane potential and diminished mitochondrial respiration. The addition of antioxidant NAC prevented the decrease of basal and substrate-induced respiration seen in LPON-treated cells, thus supporting the role of ROS in modulating mitochondrial function in nutrient perturbation (35, 36). Taken together, these results indicate an inhibition of oxidative phosphorylation mediated by ROS possibly on the terminal components of mitochondrial respiratory chain, cytochrome c oxidase (complex IV). ROS and high fat diet have been previously shown to diminish cytochrome c oxidase activity leading to an increase in $NADH/NAD^+$ with concomitant high mitochondrial membrane potential (37, 38). Therefore, it is plausible that enhanced ROS is responsible for the ensemble of mitochondrial effects observed with LPON.

Akin to the findings in steatohepatitis, ROS formation in LPON-treated cells was not mitigated by diminished respiration (4, 39). Indeed, a dramatic rise in superoxide formation was observed with LPON, which is likely to be attributable to increased mitochondrial membrane potential (40, 41). In contrast, the treatment with oleate did not affect cell respiration and maintained a relatively low mitochondrial membrane potential, resulting in a smaller amount of superoxide formation. In addition, the intact respiration maintains constant NADH oxidation thus minimizing the ROS formation further (25). Interestingly, despite the contrasting ROS formation, mitochondrial NADH/NAD^+ ratio between LPON and the untreated cells was comparable. However, preserved mitochondrial function in the untreated cells, as evidenced by active respiration and low mitochondrial membrane potential, is likely to maintain steady flow of electrons along the mitochondrial chain necessary for an efficient NADH oxidation to NAD^+. The findings of lower cytosolic NADH/NAD^+ ratio in the untreated cells compared with LPON further support this notion. Therefore, it is plausible that the similarity in mitochondrial NADH/NAD^+ ratio reflects the differences in the rate of NADH formation from the TCA cycle. Specifically, the 72 h of LPON treatment may have led to the downregulation of TCA cycle and the observed mitochondrial NADH/NAD^+ ratio may have been normalized as part of the ensuing metabolic adaptations in the presence of mitochondrial impairment.

In support of this, the concentration of malate, a TCA cycle intermediate, was found to be significantly higher with LPON than either oleate or the untreated cells. It is possible that the surge of energy substrates and the subsequent mitochondrial impairment with LPON would initially lead to a rise in NADH/NAD^+ ratio such that it favours the conversion of oxaloacetate to malate. The lowering of oxaloacetate can dampen the TCA cycle turnover, thus diminishing the NADH formation (27). In effect, such reduction in oxaloacetate decreases its availability to condense with acetyl-coA to form citrate. Indeed, citrate levels were lower with LPON compared with oleate. Furthermore, citrate synthase activity is diminished in the presence of oxidative stress as well as in elevated NADH/NAD^+ (13, 38). The diversion of acetyl-coA towards ketogenesis is yet another classic acute metabolic adaptation to the reduction in TCA cycle activity. These adaptations are necessary in the presence of mitochondrial impairments. Excessive supply of NADH in the presence of electron flow disruption (for example, in ROS-induced mitochondrial injury) can promote further ROS formation. Although it is conceivable that reduced basal respiration observed with LPON reflects decreased NADH availability, it is unlikely that this underpins the diminished substrate-induced respiration, particularly in the presence of DNP.

Increased gluconeogenesis exemplifies an appropriate response to curb further ROS formation from excessive substrate flux into the TCA cycle. In the setting of nutrient excess, increased mitochondrial superoxide production has been proposed to be the signal that drives a cellular response to induce insulin resistance as part of the antioxidant defense mechanism (42). The findings of enhanced glucose formation in octanoate and LPO-treated cells highlight two important points. Firstly, altered glucose metabolism occurs before the onset of mitochondrial impairment. This further supports that mitochondrial alterations do not precede insulin resistance (13). Secondly, the extent of triglyceride accumulation does not correlate with glucose formation.

Whether the unperturbed respiration with oleate can be attributed to enhanced mitochondrial antioxidants remains unknown. Oleate-induced steatosis had been shown to increase cellular GSH content accompanied by enhanced lipid peroxidation (28). A major end-product of lipid peroxidation, 4-HNE, has been proposed to exert cytoprotective effect primarily through induction of TR1 (29). For this reason, we have chosen to examine the concentration of TR1 to determine whether triglyceride accumulation with oleate was accompanied by enhanced cytoprotective effect, which may potentially influence the impact of ROS on mitochondrial respiration. However, TR1 concentrations in oleate-treated cells were similar to the untreated cells.

In summary, our data suggest that hepatic steatosis per se does not have direct impact on mitochondrial function; nor does it influence glucose metabolism. It is simply a marker of deranged metabolic milieu. In contrast, ROS is a determinant of mitochondrial function in the long term. It is likely that mitochondria act as energy sensor with mitochondrial ROS providing the impetus to metabolic adaptations gearing towards limiting further ROS production. Such adaptations would include curtailing energy substrate flux into TCA cycle, thus acetyl-coA has to be diverted towards other pathways including ketogenesis and de novo lipogenesis. However, a critical juncture would be reached if the surge of energy substrates were to continue. These adaptations and antioxidants would no longer able to cope with excessive ROS formation. In this milieu, further ROS formation triggers a vicious cycle that can potentially promote the release of various proinflammatory cytokines and onset of changes favouring the progression of steatohepatitis and fibrosis (27). Thus, reduction in cellular steatosis is not always the desired outcome without concomitant reduction in energy substrate availability and ROS formation. The results of this study would support strategies focused on establishing the balance between excessive ROS production and antioxidant capacity in preventing the onset of nonalcoholic steatohepatitis.

Acknowledgements

The authors thank S. Mitchell for his assistance in electron microscopy, CALM facility, Queen's Medical Research Institute for the guidance in confocal micros-

copy, P. Cowan for her immeasurable support and assistance in this project.

Authors have no conflict of interest to declare.

References

1. Contos MJ, Sanyal AJ. The clinicopathologic spectrum and management of nonalcoholic fatty liver disease. *Adv Anat Pathol* 2002; **9**: 37–51.
2. Adams LA, Sanderson S, Lindor KD, Angulo P. The histological course of nonalcoholic fatty liver disease: a longitudinal study of 103 patients with sequential liver biopsies. *J Hepatol* 2005; **42**: 132–8.
3. Powell EE, Cooksley WG, Hanson R, *et al.* The natural history of nonalcoholic steatohepatitis: a follow-up study of forty-two patients for up to 21 years. *Hepatology* 1990; **11**: 74–80.
4. Kojima H, Sakurai S, Uemura M, *et al.* Mitochondrial abnormality and oxidative stress in nonalcoholic steatohepatitis. *Alcohol Clin Exp Res* 2007; **31**(1 Suppl.): S61–6.
5. Sanyal AJ, Campbell-Sargent C, Mirshahi F, *et al.* Nonalcoholic steatohepatitis: association of insulin resistance and mitochondrial abnormalities. *Gastroenterology* 2001; **120**: 1183–92.
6. Pessayre D, Fromenty B, Mansouri A. Mitochondrial injury in steatohepatitis. *Eur J Gastroenterol Hepatol* 2004; **16**: 1095–105.
7. Houstis N, Rosen ED, Lander ES. Reactive oxygen species have a causal role in multiple forms of insulin resistance. *Nature* 2006; **440**: 944–8.
8. Cortez-Pinto H, Chatham J, Chacko VP, *et al.* Alterations in liver ATP homeostasis in human nonalcoholic steatohepatitis: a pilot study. *JAMA* 1999; **282**: 1659–64.
9. Raffaella C, Francesca B, Italia F, *et al.* Alterations in hepatic mitochondrial compartment in a model of obesity and insulin resistance. *Obesity (Silver Spring)* 2008; **16**: 958–64.
10. Perez-Carreras M, Del Hoyo P, Martin MA, *et al.* Defective hepatic mitochondrial respiratory chain in patients with nonalcoholic steatohepatitis. *Hepatology* 2003; **38**: 999–1007.
11. Caldwell SH, Swerdlow RH, Khan EM, *et al.* Mitochondrial abnormalities in non-alcoholic steatohepatitis. *J Hepatol* 1999; **31**: 430–4.
12. Marchesini G, Bugianesi E, Forlani G, *et al.* Nonalcoholic fatty liver, steatohepatitis, and the metabolic syndrome. *Hepatology* 2003; **37**: 917–23.
13. Bonnard C, Durand A, Peyrol S, *et al.* Mitochondrial dysfunction results from oxidative stress in the skeletal muscle of diet-induced insulin-resistant mice. *J Clin Invest* 2008; **118**: 789–800.
14. Wang T, Si Y, Shirihai OS, *et al.* Respiration in adipocytes is inhibited by reactive oxygen species. *Obesity (Silver Spring)* 2009; **18**: 1493–502.
15. Kumar S, Sitasawad SL. N-acetylcysteine prevents glucose/glucose oxidase-induced oxidative stress, mitochondrial damage and apoptosis in H9c2 cells. *Life Sci* 2009; **84**: 328–36.
16. Guo W, Choi JK, Kirkland JL, Corkey BE, Hamilton JA. Esterification of free fatty acids in adipocytes: a comparison between octanoate and oleate. *Biochem J* 2000; **349** (Part 2): 463–71.
17. Sussman NL, Gislason GT, Conlin CA, Kelly JH. The Hepatix extracorporeal liver assist device: initial clinical experience. *Artif Organs* 1994; **18**: 390–6.
18. Filippi C, Keatch SA, Rangar D, *et al.* Improvement of C3A cell metabolism for usage in bioartificial liver support systems. *J Hepatol* 2004; **41**: 599–605.
19. Clarke C, Baghdadi H, Howie AF, *et al.* Selenium supplementation attenuates procollagen-1 and interleukin-8 production in fat-loaded human C3A hepatoblastoma cells treated with TGFbeta1. *Biochim Biophys Acta* 2010; **1800**: 611–8.
20. Kaiser S, Gerok W, Haussinger D. Ammonia and glutamine metabolism in human liver slices: new aspects on the pathogenesis of hyperammonaemia in chronic liver disease. *Eur J Clin Invest* 1988; **18**: 535–42.
21. Choi YS, Lee DY, Kim IY, *et al.* Ammonia removal using hepatoma cells in mammalian cell cultures. *Biotechnol Prog* 2000; **16**: 760–8.
22. Miller S, Walker SW, Arthur JR, *et al.* Selenite protects human endothelial cells from oxidative damage and induces thioredoxin reductase. *Clin Sci* 2001; **100**: 543–50.
23. Bergmeyer H. *Methods of Enzymatic Analysis*. London: Academic Press, 1974.
24. Nakamura S, Takamura T, Matsuzawa-Nagata N, *et al.* Palmitate induces insulin resistance in H4IIEC3 hepatocytes through reactive oxygen species produced by mitochondria. *J Biol Chem* 2009; **284**: 14809–18.
25. Seo BB, Marella M, Yagi T, Matsuno-Yagi A. The single subunit NADH dehydrogenase reduces generation of reactive oxygen species from complex I. *FEBS Lett* 2006; **580**: 6105–8.
26. Murphy MP. How mitochondria produce reactive oxygen species. *Biochem J* 2009; **417**: 1–13.
27. Wang Q, Yu L, Yu CA. Cross-talk between mitochondrial malate dehydrogenase and the cytochrome bc1 complex. *J Biol Chem* 2010; **285**: 10408–14.
28. Garcia MC, Amankwa-Sakyi M, Flynn TJ. Cellular glutathione in fatty liver *in vitro* models. *Toxicol In Vitro* 2011; **25**: 1501–6.
29. Chen ZH, Saito Y, Yoshida Y, *et al.* 4-Hydroxynonenal induces adaptive response and enhances PC12 cell tolerance primarily through induction of thioredoxin reductase 1 via activation of Nrf2. *J Biol Chem* 2005; **280**: 41921–7.
30. Moon S, Fernando MR, Lou MF. Induction of thioltransferase and thioredoxin/thioredoxin reductase systems in cultured porcine lenses under oxidative stress. *Invest Ophthalmol Vis Sci* 2005; **46**: 3783–9.
31. Handy DE, Lubos E, Yang Y, *et al.* Glutathione peroxidase-1 regulates mitochondrial function to modulate redox-dependent cellular responses. *J Biol Chem* 2009; **284**: 11913–21.
32. Nagaya T, Tanaka N, Suzuki T, *et al.* Down-regulation of SREBP-1c is associated with the development of burned-out NASH. *J Hepatol* 2010; **53**: 724–31.
33. Gottschalk S, Zwingmann C. Altered fatty acid metabolism and composition in cultured astrocytes under hyperammonemic conditions. *J Neurochem* 2009; **109**(Suppl. 1): 258–64.
34. Listenberger LL, Han X, Lewis SE, *et al.* Triglyceride accumulation protects against fatty acid-induced lipotoxicity. *Proc Natl Acad Sci USA* 2003; **100**: 3077–82.
35. Kohli R, Pan X, Malladi P, Wainwright MS, Whitington PF. Mitochondrial reactive oxygen species signal hepatocyte

steatosis by regulating the phosphatidylinositol 3-kinase cell survival pathway. *J Biol Chem* 2007; **282**: 21327–36.
36. Nulton-Persson AC, Szweda LI. Modulation of mitochondrial function by hydrogen peroxide. *J Biol Chem* 2001; **276**: 23357–61.
37. Paradies G, Petrosillo G, Pistolese M, Ruggiero FM. The effect of reactive oxygen species generated from the mitochondrial electron transport chain on the cytochrome c oxidase activity and on the cardiolipin content in bovine heart submitochondrial particles. *FEBS Lett* 2000; **466**: 323–6.
38. Vial G, Dubouchaud H, Couturier K, *et al.* Effects of a high-fat diet on energy metabolism and ROS production in rat liver. *J Hepatol* 2011; **54**: 348–56.
39. Vendemiale G, Grattagliano I, Caraceni P, *et al.* Mitochondrial oxidative injury and energy metabolism alteration in rat fatty liver: effect of the nutritional status. *Hepatology* 2001; **33**: 808–15.
40. Skulachev VP. Role of uncoupled and non-coupled oxidations in maintenance of safely low levels of oxygen and its one-electron reductants. *Q Rev Biophys* 1996; **29**: 169–202.
41. Votyakova TV, Reynolds IJ. DeltaPsi(m)-dependent and -independent production of reactive oxygen species by rat brain mitochondria. *J Neurochem* 2001; **79**: 266–77.
42. Hoehn KL, Salmon AB, Hohnen-Behrens C, *et al.* Insulin resistance is a cellular antioxidant defense mechanism. *Proc Natl Acad Sci USA* 2009; **106**: 17787–92.
43. Abiru S, Migita K, Maeda Y, *et al.* Serum cytokine and soluble cytokine receptor levels in patients with non-alcoholic steatohepatitis. *Liver Int* 2006; **26**: 39–45.

Supporting Information

Additional Supporting Information may be found in the online version of this article:

Data S1. The concentrations of lactate, pyruvate, acetoacetate and -hydroxybutyrate.

Please note: Wiley-Blackwell are not responsible for the content or functionality of any supporting materials supplied by the authors. Any queries (other than missing material) should be directed to the corresponding author for the article.